Nanoscale Advances

ROYAL SOCIETY OF CHEMISTRY

PAPER

View Article Online
View Journal | View Issue

Cite this: *Nanoscale Adv.*, 2025, **7**, 5104

A new MIL-101-type chromium-based metal–organic framework with densely packed sulfonic groups: an ultra-high uptake of toxic Pb^{2+} and Cu^{2+} ions from an aqueous medium†

My V. Nguyen, *[a] Huy K. Duong,[a] Hung N. Nguyen,[a] Loc C. Luu[b] and Thai M. Nguyen[a]

Metal–organic frameworks have been demonstrated to be effective adsorbents of heavy metal ions in recent decades. Nevertheless, their practical applications remain limited because of their slow uptake rates and a lack of functionalization techniques. To overcome these drawbacks, a new sulfonic-functionalized chromium-based metal–organic framework with a MIL-101-type structure was successfully fabricated, termed MIL-101-SO_3H(N), *via* a solvothermal procedure, and it demonstrated a unique uptake ability for highly toxic Pb^{2+} and Cu^{2+} cations from solution. Accordingly, MIL-101-SO_3H(N) demonstrated the highest adsorption capacity of 1449.7 mg g^{-1} and 1328.4 mg g^{-1} for Pb^{2+} and Cu^{2+} ions, respectively, which are much higher than those of previously reported adsorbents. It is noteworthy that the obtained data of heavy metal ion adsorption over MIL-101-SO_3H(N) best fit with the pseudo-second-order kinetic and Langmuir isothermal models, indicating that chemisorption occurred during the uptake process. In particular, the effective uptake of Pb^{2+} and Cu^{2+} ions is depicted by the strong electrostatic interaction between the positively charged metal ions and negatively charged sulfonate groups inside the MOF backbone as well as the large and suitable pore sizes of the material, leading to a considerable enhancement of metal ion uptake from an aqueous medium. These findings illustrate that the new SO_3H-modified Cr-based MOF is a potential candidate for use as an efficient absorbent in eliminating highly toxic heavy metal ions under practical conditions.

Received 4th May 2025
Accepted 26th June 2025

DOI: 10.1039/d5na00442j

rsc.li/nanoscale-advances

1 Introduction

With the rapid development of industrialization and modernization, highly toxic heavy metal ions are released into the environment without proper treatment, resulting in potential risks to human health and aquatic life underwater. Heavy metal ions, especially Pb^{2+} and Cu^{2+}, are widely utilized in industrial fields, including construction and light industry, painting, pigments, and battery technology.[1–3] Accordingly, wastewater containing even low concentrations of Pb^{2+} and Cu^{2+} ions can cause serious health threats, such as cancer, kidney damage, immune system imbalance, and functional disorders of the heart and brain.[4–8] Therefore, it is urgent to seek efficient removal solutions for poisonous heavy metal ions before releasing them into the water medium. Different techniques to eliminate heavy metal ions involve ion exchange,[9,10] electrochemical treatment,[11] chemical precipitation,[12,13] and adsorption.[13,14] Among these, adsorption is admitted as one of the most effective procedures to remove heavy metal ions from the aqueous medium due to its uncomplicated design, facile manipulation, high uptake, and versatility.[15–18] Various adsorptive materials have been employed to eliminate toxic metal ions from water, including composite/inorganic materials,[19–21] activated carbon,[22,23] clay,[24] and zeolite.[25,26] Nevertheless, many obstacles were observed in using these materials to treat heavy metal ions from wastewater in the aspects of complicated functionalization, low efficiency, and slow uptake rate because there is no strong and effective interaction between the adsorbent and guest-heavy metal ions. Thus, scientists have focused on designing and constructing novel alternative adsorptive materials, possessing extraordinary performances to overcome the mentioned limitations and efficiently apply them in practical situations. In recent decades, metal–organic frameworks (MOFs) have received much attention in capturing heavy metal ions from wastewater[27–29] due to their unique properties, such as large porous volume, high specific surface area, low density, and high chemical and thermal robustness.[30,31] Herein, MOFs are constructed from

[a]*Faculty of Chemistry, Ho Chi Minh City University of Education, Ho Chi Minh City, 700000, Vietnam. E-mail: mynv@hcmue.edu.vn*

[b]*HCMC University of Technology, VNU-HCM, 268 Ly Thuong Kiet, District 10, Ho Chi Minh City, 700000, Vietnam*

† Electronic supplementary information (ESI) available: Full synthesis and characterization details. See DOI: https://doi.org/10.1039/d5na00442j

organic ligands and inorganic metal clusters to produce a three-dimensional architecture with various topologies. In particular, the flexible backbone of MOFs facilitates effortless functionalization of organic linkers, driving various applications in fields, such as catalysis,[32,33] adsorption,[34,35] sensing,[36,37] and energy storage.[38,39] In addition, Cr-based MOFs are well-known for their large pore volume and high water stability, properties that have been widely investigated to enhance the removal of heavy metal ions. In detail, MIL-101(Cr) with a large specific surface area exhibited efficient adsorption of Cu^{2+}, Cd^{2+}, and Pb^{2+} in solution.[40] Moreover, modifying the organic backbone of the MOF material with rich-electron moieties, such as thiol, amino, hydroxyl, and carboxyl groups, can enhance its uptake capacity for Pb^{2+} and Cu^{2+} ions *via* electron donor–acceptor interactions, forming stable complexes. For example, Zhao *et al.* fabricated a Zr-based MOF with carboxyl groups, displaying a maximum adsorption capacity of 420.2 mg g^{-1} for Pb^{2+}.[41] Subramaniyam *et al.* successfully prepared an amino-modified MOF, exhibiting a Cu^{2+} uptake capacity of 125.0 mg g^{-1}.[42] Furthermore, mixed-ligand-based MOFs and MOF composites exhibited unexpectedly high uptake capacities for heavy metal ions.[43–47] Specifically, in our previous report, VNU-23 has a densely packed distribution of sulfonate moieties (SO_3^-) within the architecture, which can strongly interact with Pb^{2+} ions through electrostatic attraction, leading to a high uptake ability for Pb^{2+} (*ca.* 617.3 mg g^{-1}).[48] Consequently, the large pore diameter combined with functional groups incorporated into the MOF material significantly boosts the removal efficiency and rate of Pb^{2+} and Cu^{2+} ions from the aqueous medium. With this in mind, if a new Cr-MOF material is successfully synthesized with large cavities and negatively charged sulfonic groups within the structure, it could considerably improve the adsorption capacity and rate of heavy metal ions. This is a new approach to overcome the drawbacks of traditional adsorbents and serve the demands of real-life conditions in terms of economic efficiency and high treatment performance.

With all of this taken into account, a research plan is proposed focusing on constructing a MOF platform that affords effective adsorption of heavy metal ions with the following combined factors: (i) design of a Cr-based MOF possessing a suitable pore size and high chemical and thermal stability to operate under practical conditions effectively; (ii) introducing a large number of sulfonic moieties onto the MOF structure to efficiently interact with positively charged metal ions *via* electrostatic attraction; and (iii) evaluation of adsorption possibility of heavy metal ions and interpretation of uptake mechanisms over the fabricated MOF. Hence, in this contribution, a new Cr-MOF containing sulfonic groups, namely MIL-101-SO_3H(N), was successfully prepared to efficiently remove the highly toxic heavy metal ions of Pb^{2+} and Cu^{2+} *via* strong electrostatic attraction and appropriate pore structure. Accordingly, MIL-101-SO_3H(N) exhibited an excellent adsorption capacity of 1449.7 mg g^{-1} for Pb^{2+} and 1328.4 mg g^{-1} for Cu^{2+}, with the uptake efficiency maintained even after eight consecutive cycles. Particularly, the structural features of the material and the adsorption mechanism of Pb^{2+} and Cu^{2+} over MIL-101-SO_3H(N) were interpreted through combined modern analytical methods. These observations show that the sulfonic-functionalized Cr-based MOF is a promising adsorbent that effectively captures poisonous heavy metal ions from wastewater with great uptake capacity and rapid adsorption rate.

2 Experimental section

2.1 Starting chemicals and procedures

All the utilized chemicals, including chromium(III) nitrate nonahydrate ($Cr(NO_3)_3 \cdot 9H_2O$, 98%), 1,4-naphthalenedicarboxylic acid (1,4-H_2NDC, 98%), sulfuric acid fuming (25%), hydrochloric acid (HCl, 37%), hydrofluoric acid (HF, 98%), lead(II) nitrate ($Pb(NO_3)_2$, 99%), copper(II) sulfate ($CuSO_4 \cdot 5H_2O$, 98%), acetone (99%), and ethanol (EtOH, 99%) were obtained from local vendors and used without further purification. Water employed in this study was double distilled and filtered through a Millipore membrane.

Raman spectra were recorded using a spectrometer (XploRA ONE 532 nm, Horiba). Fourier transform infrared (FT-IR) spectra were recorded using a spectrophotometer (FT/IR-6600, Jasco) with the Attenuated Total Reflectance (ATR) sampling procedure. Powder X-ray diffraction (PXRD) measurements were carried out using a Bruker D8 Advance diffractometer using Ni-filtered Cu Kα (λ = 1.54718 Å). The 2θ range was 3–50° with a step size of 0.02° and a fixed counting time of 0.35 s per step. Thermal gravimetric (TG) analysis combined with differential scanning calorimetry (DSC) was performed using a thermal analyzer at a rate of 10 °C min^{-1} under dry air (Labsys Evo 1600 TGA, SETARAM), over a temperature range of 25–800 °C at a constant rate of 10 °C min^{-1}. Scanning electron microscopy (SEM) images were collected using a microscope (FESEM S-4800, Hitachi) at an accelerating voltage of 10 kV, coupled with energy-dispersive X-ray (EDX) mapping conducted on an instrument (EDX H-7593, Horiba). Transmission electron microscopy (TEM) images were obtained using a microscope (Jeon 1010, Hitachi) at a high voltage of 80 kV. ^{1}H-NMR spectroscopy was carried out using an NMR spectrometer (Advance Neo-600 MHz, Bruker). X-ray photoelectron spectroscopy (XPS) was conducted using an X-ray photoelectron spectrometer (PHI 5000, Chigasaki) equipped with a monochromatic Al Kα source operating at 50 W and 15 kV. Atomic absorption spectrophotometry (AAS) was performed using a spectrometer (iCE 300 Series, Thermo Scientific) with an absorption wavelength of 217 nm for Pb^{2+} and 324.7 nm for Cu^{2+}.

2.2 Synthesis of the 6-sulfonaphthalene-1,4-dicarboxylic acid linker (H_3SNAA)

According to a previously reported study,[49] a mixture of 1,4-naphthalene dicarboxylic acid (1 g, 4.63 mmol) and 5 mL of sulfuric acid fuming (10 wt%) was introduced into a 100 mL glass flask and then stirred, refluxed, and heated at 130 °C for 24 h. After cooling to room temperature, the solid was dissolved in 50 mL of distilled water, filtered, and precipitated with 10 mL of concentrated HCl. Then, the product was filtered, washed with 50 mL of concentrated HCl, and dried at 100 °C under vacuum for 24 h to obtain the pure linker, denoted as H_3SNAA.

^{1}H-NMR (DMSO-d_6, 600 Hz): δ = 9.01 (s, 1H); 8.75 (s, 1H); 8.11 (d, 2H); and 7.91 ppm (s, 1H) (Fig. S1†).

2.3 Synthesis of MIL-101-SO_3H(N)

A mixture of $Cr(NO_3)_3 \cdot 9H_2O$ (0.2664 g, 0.666 mmol) and H_3SNAA (0.3944 g, 1.332 mmol) was added to a 20 mL vial containing H_2O (4 mL) and HF (85.1 μL), and ultrasonicated for 15 min. The mixture was then transferred to a 25 mL Teflon stainless steel vessel and heated at 190 °C for 24 h. Next, the mixture was cooled to room temperature, centrifugated, and sequentially washed with H_2O (50 mL in 48 h), EtOH (50 mL in 48 h), and acetone (50 mL in 48 h). Finally, the solid was dried and activated under vacuum at 120 °C for 24 h to obtain a dark green powder (88% yield, based on Cr^{3+}), termed MIL-101-SO_3H(N).

2.4 Adsorption investigations

The pH values of the Pb^{2+} and Cu^{2+} solutions were controlled with 0.1 M NaOH and 0.1 M HCl solutions with the pH ranges of 1–5.5 (for Pb^{2+}) and 1–5.0 (for Cu^{2+}) to prevent the formation of precipitation species of Pb^{2+} and Cu^{2+}.[50–52] Pb^{2+} and Cu^{2+} uptake studies were performed with a constant stirring rate (400 rpm) at room temperature. To explore the pH_{pzc} parameter of the material, the MIL-101-SO_3H(N) sample (150 mg) was introduced into 100 mL flasks containing 50 mL of NaCl solutions (0.01 M) with different initial pH values from 2 to 12. Subsequently, the systems were stirred at room temperature for 48 h and centrifugated to separate the solid. The final pH value of the solutions after centrifugation was measured. The intersection point between the original and final pH values revealed the pH_{pzc} parameter. The concentration of Pb^{2+} and Cu^{2+} after adsorption over MIL-101-SO_3H(N) was measured using an atomic absorption spectrophotometer with an absorption wavelength of 217 nm and 324.7 nm, respectively. The adsorption capacity (mg g^{-1}) and removal efficiency (%) at intervals (q_t) and equilibrium (q_e) of the heavy metal ions were determined using the following equations:

$$q_e = \frac{C_0 - C_e}{m} \times V \quad (1)$$

$$\text{Removal efficiency} = \frac{C_0 - C_t}{C_0} \times 100 \quad (2)$$

$$q_t = \frac{C_0 - C_t}{m} \times V \quad (3)$$

where C_0, C_e, and C_t (mg L^{-1}) are the heavy metal ion concentrations at original, equilibrium, and t time. m (mg) is the MOF content, and V (mL) symbolizes the volume of the solution.

Varying amounts of MOF (5–30 mg) were added to the highly toxic heavy metal ion solutions with a specific concentration (50 mg L^{-1}) to determine the optimal dosage. Adsorption isothermal experiments were conducted using the optimal dosage, which was introduced into 100 mL of various initial concentrations of the heavy metal ions (100–1000 mg L^{-1}) at the optimal pH value and stirred for 24 h. Pb^{2+} and Cu^{2+} uptake kinetic investigations over MIL-101-SO_3H(N) were performed. In detail, 5 mg of MIL-101-SO_3H(N) was added to 50 mL of Pb^{2+} and Cu^{2+} solutions (40 mg L^{-1}) at pH = 5, and the mixtures were stirred at intervals from 1 to 20 min. Herein, the content of 5 mg and pH = 5 are selected to study the kinetics because the uptake rate of the material is rapid with the MOF content and pH over

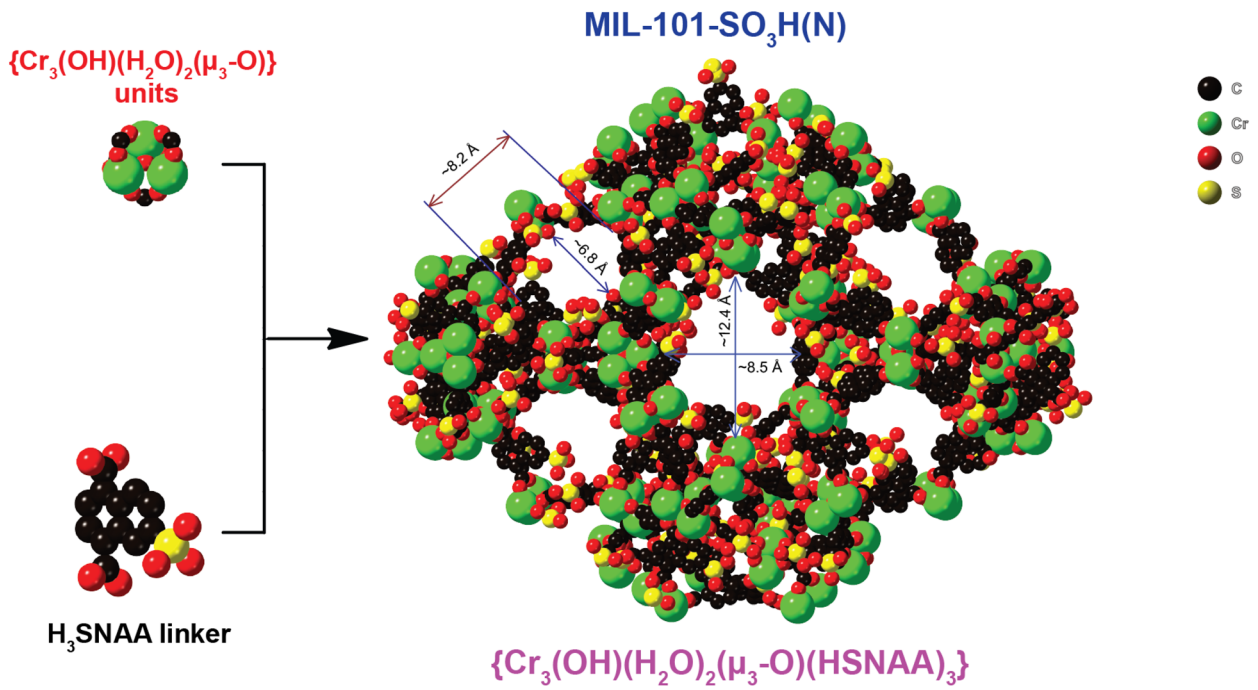

Fig. 1 The backbone of MIL-101-SO_3H(N) is generated from the {$Cr_3(OH)(H_2O)_2(\mu_3\text{-}O)$} SBUs with H_3SNAA. Atom colors: Cr polyhedra, green; C, black; O, red; S, yellow. All H atoms are omitted for clarity.

5 mg and 5, resulting in inaccurate measurement in a short interval.

The reusability of MIL-101-SO_3H(N) was studied by using 1% HNO_3 solution as an effective desorption medium. Accordingly, after removing the heavy metal ions, the sample was isolated by centrifugation, soaked in 1% HNO_3 solution, and stirred for 24 h. To further evaluate the removal efficiency of Pb^{2+} and Cu^{2+} ions from the MOF material, the filtrate was analyzed by AAS, which showed no traces of heavy metal ions. Next, MIL-101-SO_3H(N) was centrifugated, washed with excess distilled water until pH = 7, and exchanged in EtOH and acetone solvents for 24 h, respectively. The sample was then separated by

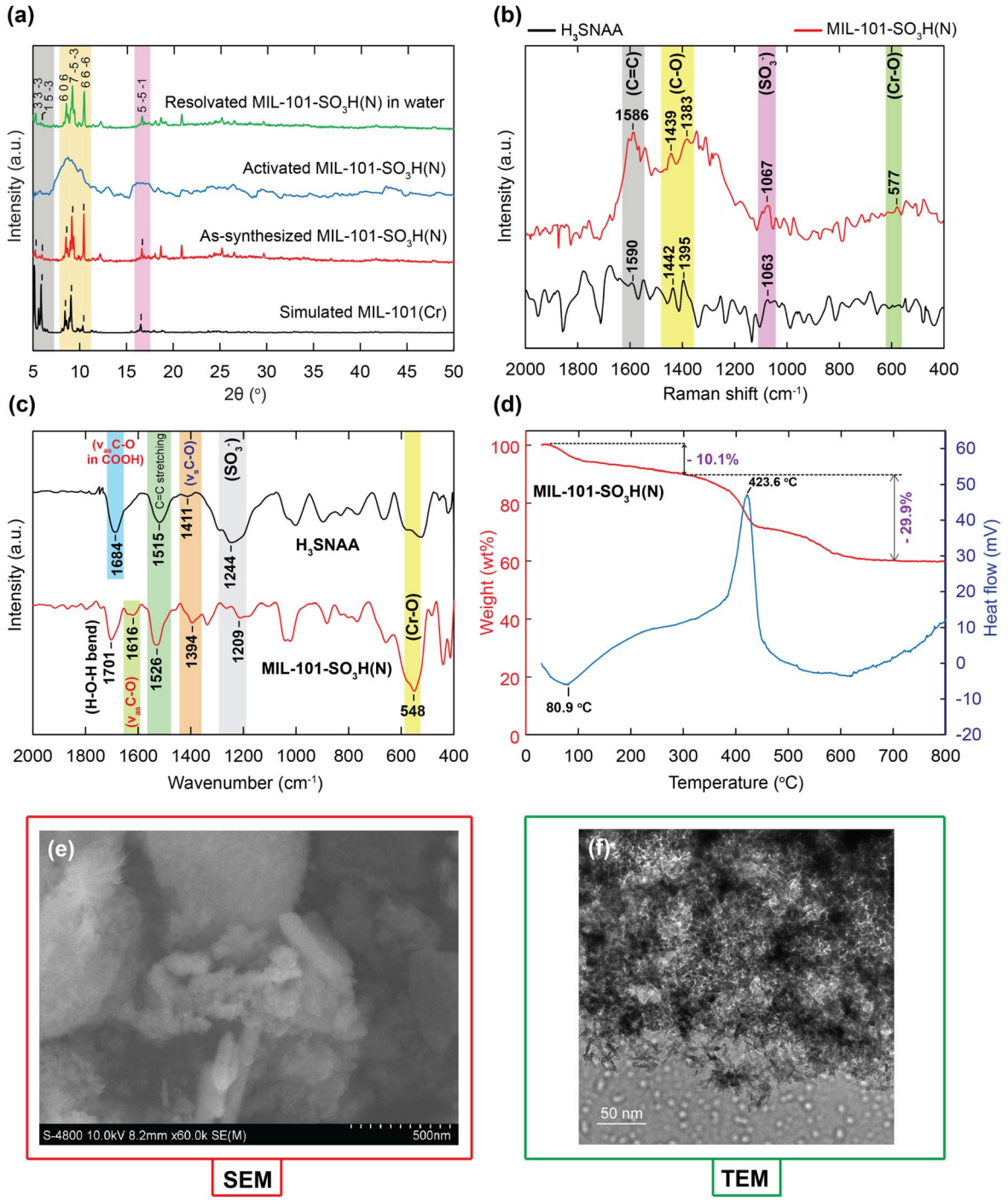

Fig. 2 Powder X-ray diffraction patterns of as-synthesized MIL-101-SO_3H(N) (red), activated MIL-101-SO_3H(N) (blue), and resolvated MIL-101-SO_3H(N) immersed in H_2O (green) in comparison with the simulated MIL-101(Cr) (black) (a); Raman spectra of MIL-101-SO_3H(N) (red) in comparison with the H_3SNAA linker (black) (b); Fourier transform infrared spectra of the H_3SNAA linker (black) and activated MIL-101-SO_3H(N) (red) (c); TGA curve (red) and DSC diagram (blue) of activated MIL-101-SO_3H(N) (d); SEM image of MIL-101-SO_3H(N) at a scale bar of 500 nm (e); TEM image of activated MIL-101-SO_3H(N) at a scale bar of 50 nm (f).

centrifugation, dried at 120 °C under a dynamic vacuum for 24 h, and employed for subsequent uptake investigations.

3 Results and discussion

3.1 Full characterization of MIL-101-SO_3H(N)

To confirm the extraordinary adsorption properties of Pb^{2+} and Cu^{2+} over the MOF backbone, a MOF design strategy is proposed based on the following incorporated factors: (a) MOFs with large cavities will support the rapid and efficient mobility of the heavy metal ions into internal pore walls, significantly enhancing the removal capacity and rate; (b) the dense distribution of sulfonic groups within the MOF architecture to generate negatively charge moieties *via* deprotonation, resulting in strong attraction with the Pb^{2+} and Cu^{2+} ions through electrostatic interactions; (c) high chemical and thermal

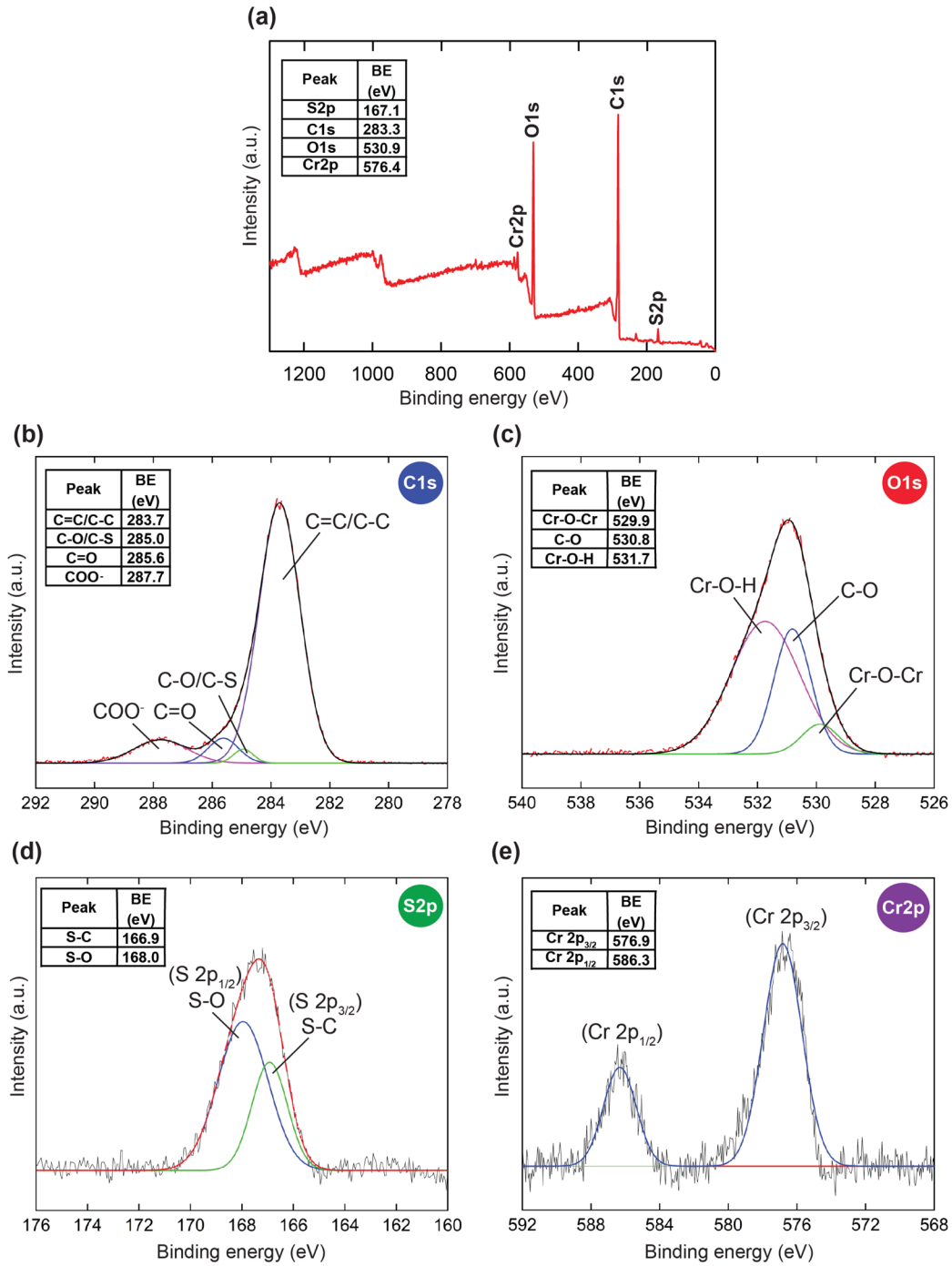

Fig. 3 The XPS analysis of MIL-101-SO_3H(N): the XPS survey of MIL-101-SO_3H(N) (red) (a); high-resolution spectrum of C 1s in MIL-101-SO_3H(N) (b); high-resolution spectrum of O 1s in MIL-101-SO_3H(N) (c); high-resolution spectrum of S 2p in MIL-101-SO_3H(N) (d); high-resolution spectrum of Cr 2p in MIL-101-SO_3H(N) (e).

stability to ensure performance under harsh practical conditions. With all this in mind, a mixture of $Cr(NO_3)_3 \cdot 9H_2O$ salt and the H_3SNAA linker was dissolved in water as a mild solvent in the presence of hydrofluoric acid and heated at 190 °C for 24 h to obtain a dark green powder, termed MIL-101-SO_3H(N) (Fig. 1). Next, the solid was sequentially washed with water, ethanol, and acetone, to remove any residual precursors. The sample was then dried under dynamic vacuum at 120 °C for 24 h to remove the solvents from the MOF structure. It is noteworthy that MIL-101-SO_3H(N) is constructed from trinuclear $\{Cr_3(OH)(H_2O)_2(\mu_3\text{-}O)\}$ building units and bridging 6-sulfonaphthalene-1,4-dicarboxylate ligands to generate pentagonal and hexagonal windows measuring 6.8 × 8.2 Å and 8.5 × 12.4 Å in diameter, which are combined into mesoporous cages (Fig. 1). The window diameters of the structure were measured using CrystalMarker version 10.8 software, considering the van der Waals radii of the atoms. These pore window values agree with the pore distribution analysis of MIL-101-SO_3H(N) (Fig. S2†). Interestingly, MIL-101-SO_3H(N) possesses densely packed SO_3H groups and appropriate pore diameters, driving efficient capture of the heavy metal ions onto the MOF backbone *via* electrostatic attraction between the negatively charged sulfonate moieties and the heavy metal cations, the selectivity of which is governed by the window pore size. Additionally, to evaluate the influence of the sulfonic groups on the adsorption capacity of the Pb^{2+} and Cu^{2+} ions, we prepared a Cr-based MOF with a structure similar to that of MIL-101-SO_3H(N), denoted as MIL(Cr)-Z1. MIL(Cr)-Z1 was synthesized by blending Cr^{3+} salt and the non-SO_3H-modified 1,4-H_2NDC linker in H_2O solvent in the presence of a mixture of acetic acid and HF as the modulators to support the crystal growth process, and the mixture was heated at 210 °C for 10 h.[53]

The single-phase level of MIL-101-SO_3H(N) was determined by powder X-ray diffraction (PXRD) measurement, which is in high accordance with the simulated structure based on lattice planes such as (3 3 −3), (1 5 −3), (6 0 6), (7 −5 −3), (6 6 −6), (5 −5 −1) (Fig. 2a). In particular, the crystallinity of MIL-101-SO_3H(N) is decreased during the activation process. This can be attributed to the strong interaction between the solvent molecules and the sulfonic groups *via* hydrogen bond networks, resulting in a structural order decline upon activation due to the release of guest molecules from the framework. This

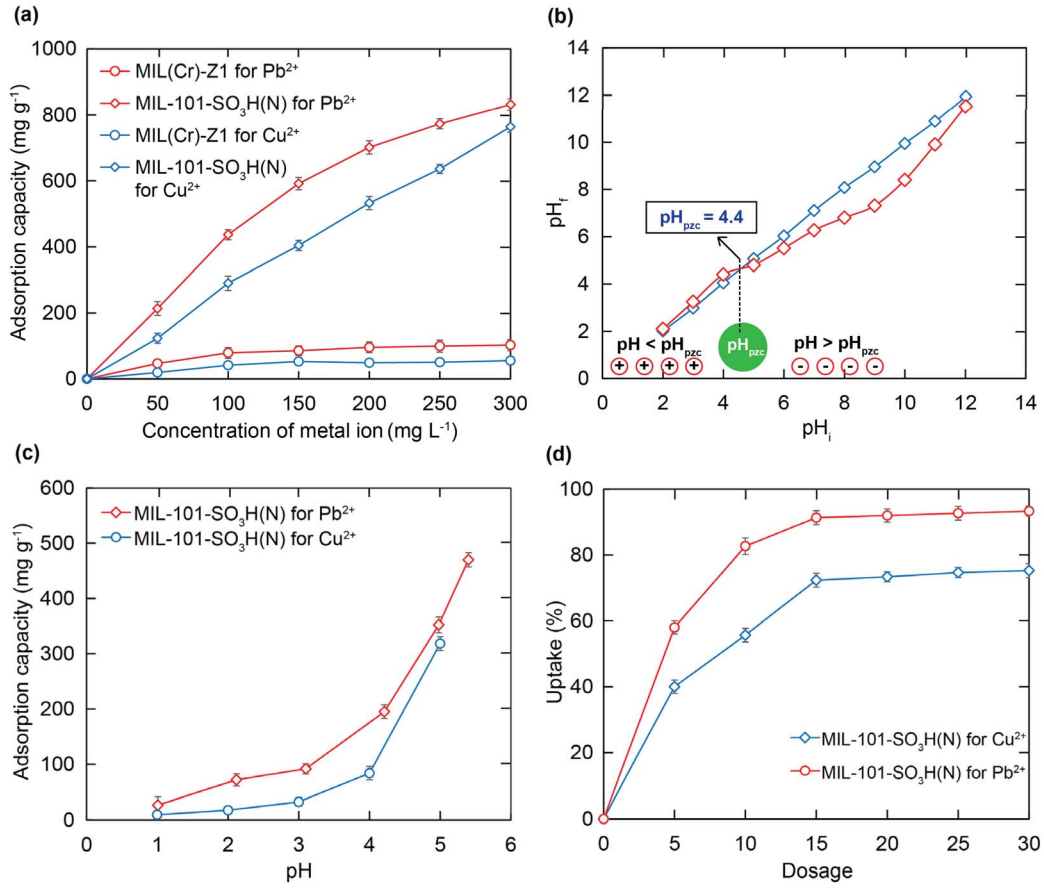

Fig. 4 Effect of the amount of SO_3H groups within the structures of MIL(Cr)-Z1 and MIL-101-SO_3H(N) on the Pb^{2+} and Cu^{2+} uptake capacity (a) [m = 10 mg, V = 100 mL, C_0 = 50–300 mg L^{-1}, t = 24 h, pH = 5]; the dependence of the original pH on the final pH for calculating pH_{pzc} (b); influence of solution pH on the adsorption capacity of Pb^{2+} and Cu^{2+} over MIL-101-SO_3H(N) at different concentrations of Pb^{2+} and Cu^{2+} (c) [m = 10 mg, V = 100 mL, C_0 = 250 mg L^{-1}, t = 24 h, pH = 1–5.5 for the Pb^{2+} uptake and pH = 1–5 for the Cu^{2+} uptake]; influence of MIL-101-SO_3H(N) content on the Pb^{2+} and Cu^{2+} uptake (d) [m = 5–30 mg, V = 100 mL, C_0 = 50 mg L^{-1}, t = 24 h, pH = 5.5 for the Pb^{2+} uptake and pH = 5 for the Cu^{2+} uptake].

phenomenon is also observed in the N_2 adsorption measurement at 77 K for the activated MIL-101-SO_3H(N) (Fig. S2†). Accordingly, the Langmuir and BET surface areas are 337.5 and 263.8 $m^2\ g^{-1}$, respectively, which are much smaller than the specific surface values of non-SO_3H-functionalized MIL(Cr)-Z1.[53] The phenomenon is similar to that reported in previously published studies.[32–34] Interestingly, the architectural order is restored after MIL-101-SO_3H(N) is immersed in water (Fig. 2a).

Furthermore, Raman spectra of activated MIL-101-SO_3H(N) and the H_3SNAA linker are clearly shown in Fig. 2b. In detail, the vibrational bands observed at 1067, 1383, 1439, and 1586 cm^{-1} in the MIL-101-SO_3H(N) spectrum correspond to the SO_3^-, C–O and C=C bonds, respectively, but appear at different wavenumbers in the H_3SNAA linker spectrum. Particularly, the characteristic signal at 577 cm^{-1} is assigned to the Cr–O absorption band in MIL-101-SO_3H(N), which is absent in the linker spectrum. Besides, the FT-IR spectra of H_3SNAA and MIL-101-SO_3H(N) are recorded and illustrated in Fig. 2c. Accordingly, vibrational modes corresponding to asymmetric C–O stretching, C=C stretching, symmetric C–O stretching, and SO_3^- groups located at 1616, 1526, 1394, and 1209 cm^{-1}, respectively, are observed in the MOF spectrum, while these bands appear at various positions in the linker spectrum. This can be explained by the formation of the coordination bonds

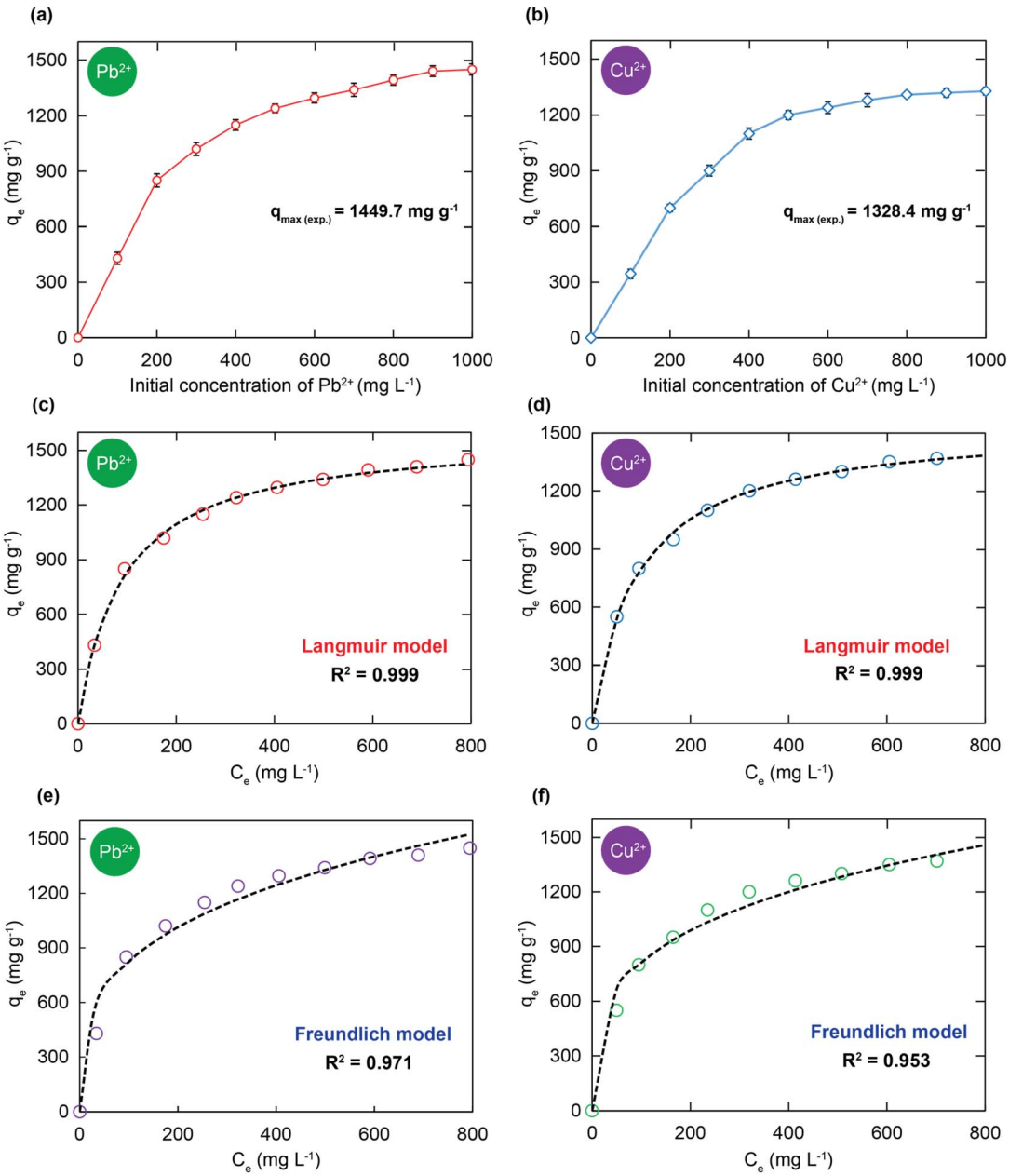

Fig. 5 Effect of initial concentration on the Pb^{2+} adsorption capacity (a), and the Cu^{2+} uptake capacity (b) over MIL-101-SO_3H(N) [$m = 15$ mg, $V = 100$ mL, $C_0 = 100–1000$ mg L^{-1}, $t = 24$ h, pH = 5.5 for the Pb^{2+} uptake, and pH = 5 for the Cu^{2+} uptake]. Data fitting with the adsorption isotherm models: Langmuir for Pb^{2+} (c), Langmuir for Cu^{2+} (d), Freundlich for Pb^{2+} (e), and Freundlich for Cu^{2+} (f).

within the MOF backbone. Notably, the Cr–O vibration is also found at 548 cm^{-1}, similar to the mentioned Raman spectrum.

To further gain insight into the features of MIL-101-SO_3H(N), TGA-DSC, SEM-EDX-mapping, TEM, and XPS analyses were carried out on the MOF sample. Accordingly, the TGA-DSC curve was recorded under dry air conditions (80% N_2 and 20% O_2) and is clearly illustrated in Fig. 2d. As a result, a weight loss of 10.1% from room temperature to 300 °C is assigned to the evaporation of surface absorbed and coordinated water molecules within the clusters of the material, owing to a maximum endothermic signal at 80.9 °C. Next, the weight loss of 29.9% with a strong exothermic signal at 423.6 °C is ascribed to the complete decomposition of the framework in the range of 300 to 700 °C. Hence, the architectural robustness of MIL-101-SO_3H(N) is indicated at about 300 °C. This shows that MIL-101-SO_3H(N) is a potential candidate for applications in practical situations. It is noteworthy that SEM and TEM measurements reveal that MIL-101-SO_3H(N) particles exhibit needle-like rod shapes with a highly uniform distribution with an average size of about 25–30 nm (Fig. 2e and f). In addition, the EDX-mapping spectrum exhibits a uniform presence of C, O, S, and Cr elements on the surface of the material (Fig. S3†). Particularly, XPS analyses display the coexistence of C, O, S, and Zr elements in MIL-101-SO_3H(N) (Fig. 3a). High-resolution spectra were utilized to assess the valence states of each element present on the surface of the material. In the high-resolution C 1s spectrum of MIL-101-SO_3H(N), different signals at 283.7, 285.0, 285.6, and 287.7 eV can be attributed to the existence of C=C/C–C, C–O/C–S, C=O, and COO^- bonds inside MIL-101-SO_3H(N) (Fig. 3b).[54–56] The O 1s curve is divided into three distinctive peaks at 529.9 eV for the Cr–O–Cr bond, 530.8 eV for the C–O bond, and 531.7 eV for the Cr–O–H bond (Fig. 3c).[57,58] Subsequently, the high-resolution S 2p spectrum indicates the characteristic signals at 166.9 and 168.0 eV, corresponding to S $2p_{3/2}$ (S–C) and S $2p_{1/2}$ (S–O), respectively (Fig. 3d).[54] Notably, the Zr core level spectra in the MOF sample show two peaks at 576.9 and 586.3 eV, corresponding to Cr $2p_{3/2}$ and Cr $2p_{1/2}$, respectively (Fig. 3e).[57,59] These findings demonstrate the efficient functionalization of sulfonic moieties onto the MOF framework and the high phase purity of the material.

3.2 Effect of sulfonic groups

A series of survey experiments were conducted to interpret the influence of the amount of sulfonic moieties inside the MOF architecture on the metal ion uptake capacity. Consequently, 10 mg of MIL-101-SO_3H(N) and non-SO_3H-functionalized MIL(Cr)-Z1 were each added to 100 mL of heavy metal ion solutions with initial concentrations ranging from 50 to 300 mg L^{-1}. In detail, the MIL(Cr)-Z1 material possesses a low adsorption capacity for Pb^{2+} (102.7 mg g^{-1}) and Cu^{2+} (55.3 mg g^{-1}) with an original metal ion concentration of 300 mg L^{-1} at pH = 5 (Fig. 4a). This poor uptake can be attributed to the lack of negatively charged SO_3^- moieties inside MIL(Cr)-Z1, causing weak interaction between the capturing sites and the metal cations. In contrast, the Pb^{2+} and Cu^{2+} uptake capacity of MIL-101-SO_3H(N) is 831.7 and 764.1 mg g^{-1} at pH = 5, respectively (Fig. 4a). It is noted that the excellent adsorption capacity of metal ions over MIL-101-SO_3H(N) is attributed to the generation of the effective electrostatic attraction between the negatively charged carriers and the Pb^{2+} and Cu^{2+} ions. Thus, we choose MIL-101-SO_3H(N) to investigate the subsequent uptake studies in this work.

3.3 Effect of pH

Solution pH is well known as a key parameter, as it considerably influences the electrostatic interactions between the MOF surface and charged moieties.[60,61] Investigations were performed to explore the pH_{pzc} of MIL-101-SO_3H(N). As indicated in Fig. 4b, the pH_{pzc} of the material is 4.4, indicating that the surface carries a positive charge below this point of zero charge and a negative charge above it. Continuously, experiments were performed to prove the effect of solution pH in a range from 1 to 5.5 for Pb^{2+} and from 1 to 5 for Cu^{2+}. It is worth noting that the precipitation of Pb^{2+} and Cu^{2+} occurs at pH values ≥6 and ≥5.5,[52,62] respectively, and they will separate from the mixture, driving difficulties in quantifying whether they appear due to precipitation or adsorption into the material. Fig. 4c shows the significant dependence of the solution pH on the adsorption capacity. In detail, in the pH region from 1 to 4 (<pH_{pzc}), relatively low adsorption levels of metal ions are observed. This can be explained by the protonation of sulfonic species within the MOF to form the $SO_3H_2^+$ states, resulting in a great repulsion of positively charged types such as metal cations, H^+ ions, and inner/external walls of MIL-101-SO_3H(N). Meanwhile, the uptake capacity of Pb^{2+} and Cu^{2+} promptly increases in a pH

Table 1 The fitting result confirmed from the adsorption isothermal models of Pb^{2+} and Cu^{2+} over MIL-101-SO_3H(N)

Isothermal models	Parameters	Value
Uptake of Pb^{2+}		
Langmuir	q_m (mg g^{-1})	1586.7
	K_L (L mg^{-1})	0.0111
	R^2	0.999
Freundlich	$1/n$	0.297
	K_F (mg g^{-1} (L g^{-1})$^{1/n}$)	210.61
	R^2	0.971
DR	K_{DR} (mg g^{-1})	0.173
	R^2	0.993
Temkin	K_T (L mg^{-1})	0.134
	β	7.813
	R^2	0.989
Uptake of Cu^{2+}		
Langmuir	q_m (mg g^{-1})	1545.1
	K_L (L mg^{-1})	0.0107
	R^2	0.999
Freundlich	$1/n$	0.281
	K_F (mg g^{-1} (L g^{-1})$^{1/n}$)	222.84
	R^2	0.953
DR	K_{DR} (mg g^{-1})	0.176
	R^2	0.992
Temkin	K_T (L mg^{-1})	0.142
	β	8.239
	R^2	0.987

range over pH_{pzc}, which can be assigned to the deprotonation process of sulfonic groups to create a high negative charge density at the surface and inside the MOF backbone, leading to effective electrostatic interaction between the Pb^{2+}/Cu^{2+} ions and MIL-101-SO_3H(N).[35,48,63] Hence, the optimal pH values, such as 5.5 for Pb^{2+} and 5 for Cu^{2+}, are selected for the subsequent studies.

3.4 Influence of the MOF dosage

To evaluate the best dosage of the material during the uptake of the metal ions, various contents of MIL-101-SO_3H(N) from 5 to 30 mg were introduced into the metal ion solutions and stirred for 24 h at the previously optimised pH. As shown in Fig. 4d, the adsorption efficiency increased from 58 to 91% for Pb^{2+} and from 40 to 72% owing to raising the dosage from 5 to 15 mg. It can be described that the number of capturing sites and adsorption spaces will rise with the increase of the MOF content, driving the efficient removal of the heavy metal ions

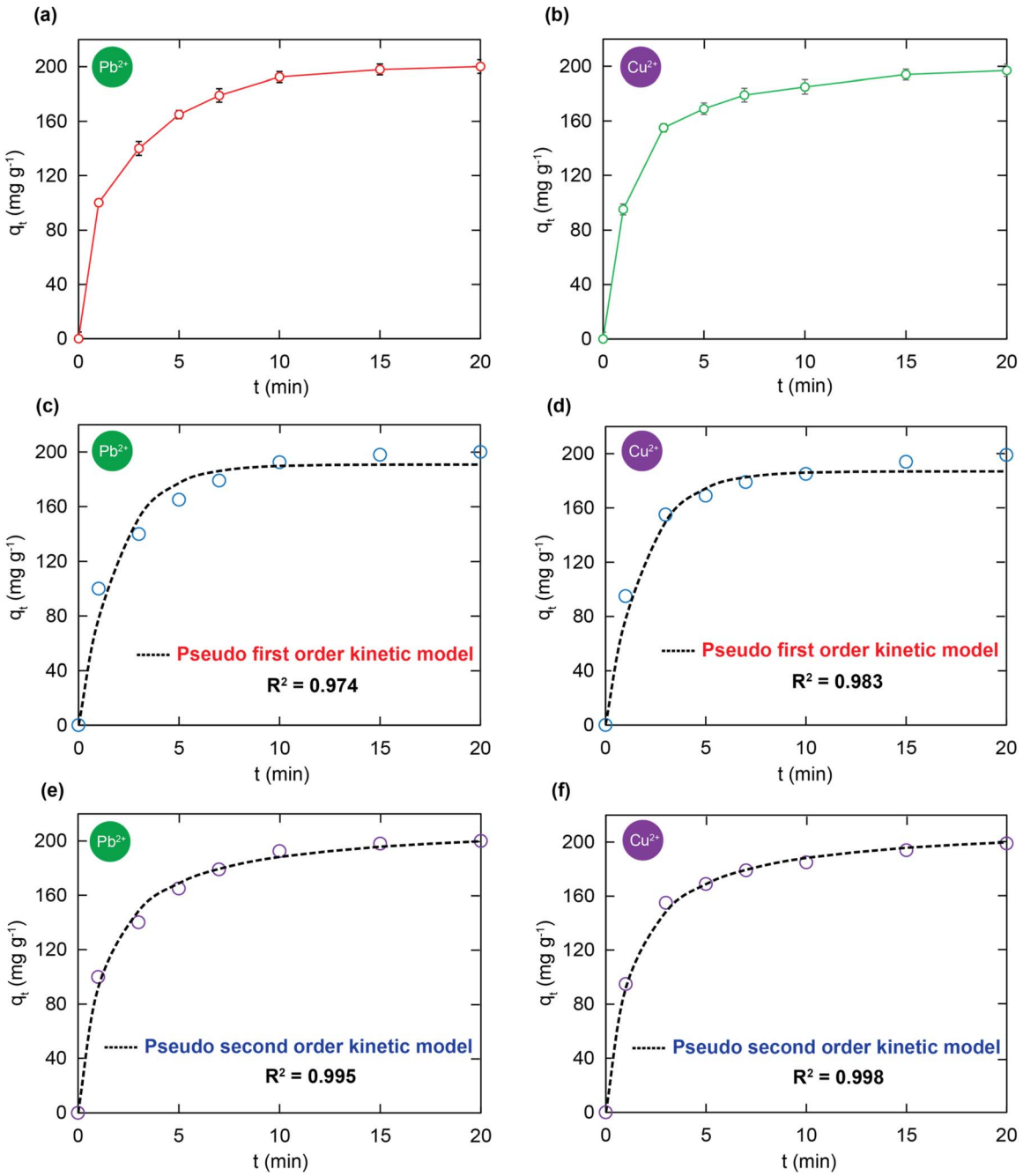

Fig. 6 The kinetic results for the Pb^{2+} (a) and Cu^{2+} (b) uptake by MIL-101-SO_3H(N) [$m = 5$ mg, $V = 50$ mL, $C_0 = 40$ mg L^{-1}, $t = 1$–20 min, pH = 5]; fitting results with the adsorption kinetic models: pseudo-first-order for Pb^{2+} (c) and for Cu^{2+} (d), pseudo-second-order for Pb^{2+} (e) and for Cu^{2+} (f).

from an aqueous medium. However, there is no significant change in the uptake of Pb^{2+} and Cu^{2+} as the MIL-101-SO_3H(N) content increases from 15 to 30 mg, indicating that the adsorption equilibrium has been reached. Therefore, the optimal dosage of 15 mg is employed for the subsequent studies.

3.5 Uptake isotherms

To explore the nature of the Pb^{2+} and Cu^{2+} uptake by MIL-101-SO_3H(N), adsorption isotherm studies were carried out. Interestingly, the dominant rise in the capturing capacity of the heavy metal ions was confirmed by the increase of the Pb^{2+} and Cu^{2+} original concentration from 100 to 1000 mg L^{-1} (Fig. 5a and b). Accordingly, the highest adsorption capacity of MIL-101-SO_3H(N) is 1449.7 mg g^{-1} for Pb^{2+} and 1328.4 mg g^{-1} for Cu^{2+}. Furthermore, to elucidate the adsorption mechanism of Pb^{2+} and Cu^{2+} onto the MOF material, isothermal models such as Langmuir, Freundlich, Dubinin-Radushkevich (DR), and Temkin were used with non-linear fittings revealed in eqn (S1)–(S4) (see Section S7†).

As illustrated in Fig. 5c–f and S4,† non-linear fitting curves and data of the uptake models for the heavy metal ion adsorption over MIL-101-SO_3H(N) are described and clearly indicated in Table 1. Consequently, the value of the non-linear fitting coefficient for the Langmuir type ($R^2 = 0.999$ for both Pb^{2+} and Cu^{2+}) is greater than those of the Freundlich ($R^2 = 0.971$ for Pb^{2+} and 0.953 for Cu^{2+}), DR ($R^2 = 0.993$ for Pb^{2+} and 0.992 for Cu^{2+}), and Temkin ($R^2 = 0.989$ for Pb^{2+} and 0.987 for Cu^{2+}) models. In particular, the theoretical adsorption capacity of the heavy metal ions determined from the intercept of the Langmuir model is 1586.7 mg g^{-1} for Pb^{2+} and 1545.1 mg g^{-1}, which are very close to the experimental data (1449.7 mg g^{-1} for Pb^{2+} and 1328.4 mg g^{-1} for Cu^{2+}). The obtained results indicate that a monolayer of Pb^{2+} and Cu^{2+} is formed at the interface between the MOF material and heavy metal ions. Additionally, it is supposed that capturing metal ions over MIL-101-SO_3H(N) is a chemisorption process based on the strong electrostatic attraction between the positively charged heavy metal ions and negatively charged SO_3^- moieties within the MOF architecture.

3.6 Adsorption kinetics

The effect of contact time on the adsorption capacity of the metal ions onto MIL-101-SO_3H(N) was investigated. Consequently, 5 mg of MIL-101-SO_3H(N) was added to 50 mL of the Pb^{2+}/Cu^{2+} solution with an initial concentration of 40 mg L^{-1} at pH = 5. To prevent incorrect measurements in the short reaction time, the pH of 5 and the content of 5 mg are selected to explore the uptake kinetics because the Pb^{2+}/Cu^{2+} adsorption rate is rapid at a higher material content and pH over 5. As illustrated in Fig. 6a and b, the removal rate of Pb^{2+} and Cu^{2+} over the MIL-101-SO_3H(N) material rises promptly in the original 5 min and reaches equilibrium after 10 min. Herein, the rapid adsorption rate is a key factor for practical applications of the material, overcoming the obstacles of the previously reported traditional materials. Besides, the uptake property is influenced by several factors, including diffusion time and chemical reaction. Kinetic models including pseudo-first-order, pseudo-second-order, and intra-particle diffusion (see the eqn (S5)–(S7) in Section S7†) were applied to obtain a deeper insight into the removal mechanism of the heavy metal ions on the MOF.

As a result, the non-linear fitting curves and data are revealed in Fig. 6c–f and Table 2. Accordingly, the non-linear fitting coefficient values of the pseudo-second-order model ($R^2 = 0.995$ for Pb^{2+} and 0.998 for Cu^{2+}) are higher than those of the pseudo-first-order model ($R^2 = 0.974$ for Pb^{2+} and 0.983 for Cu^{2+}). Thus, the adsorption of Pb^{2+} and Cu^{2+} over MIL-101-SO_3H(N) is characterized as chemisorption, indicating electron transport by the interaction between the sulfonate moieties inside the framework and the heavy metal cations.[48,64,65] It is noteworthy that, as shown in Fig. S9,† the uptake of Pb^{2+}/Cu^{2+} can be divided into three steps. In the first step, the metal ions will rapidly move to the external surface of the material from the solution. Next, the Pb^{2+}/Cu^{2+} ions diffuse into the internal channels of MIL-101-SO_3H(N), facing increased diffusion resistance. Finally, these metal ions slowly penetrate the pores of the MOF material and interact with the sulfonic groups of the backbone until the equilibrium state is established.

3.7 Regeneration investigation

The reusability of the adsorption material is considered a valuable factor in reducing product costs. Hence, the regeneration of MIL-101-SO_3H(N) in Pb^{2+} and Cu^{2+} adsorption was performed for eight consecutive cycles. As shown in Fig. 7a and b, the uptake yield was 93% for Pb^{2+} and 92% for Cu^{2+} after eight recycles without any considerable decrease in adsorption efficiency. Notably, the complete reusability of the material was confirmed by PXRD and FT-IR measurements. In detail, the PXRD patterns of MIL-101-SO_3H(N) after desorption of Pb^{2+} and Cu^{2+} ions show good agreement with those of the material before adsorption (Fig. 7c). Subsequently, the vibrational modes of MIL-101-SO_3H(N) after heavy metal ion desorption show no

Table 2 Pseudo first order and second order model parameters for the Pb^{2+} and Cu^{2+} uptake by MIL-101-SO_3H(N)

Kinetic models	Parameters	Value
Uptake of Pb^{2+}		
Pseudo first order	$q_{e,exp}$ (mg g^{-1})	199.8
	$q_{e,cal}$ (mg g^{-1})	180.8
	k_1 (min^{-1})	0.529
	R^2	0.974
Pseudo second order	$q_{e,cal}$ (mg g^{-1})	212.8
	k_2 (g mg^{-1} min^{-1})	2385
	R^2	0.995
Uptake of Cu^{2+}		
Pseudo first order	$q_{e,exp}$ (mg g^{-1})	199.1
	$q_{e,cal}$ (mg g^{-1})	177.0
	k_1 (min^{-1})	0.538
	R^2	0.983
Pseudo second order	$q_{e,cal}$ (mg g^{-1})	211.1
	k_2 (g mg^{-1} min^{-1})	2347
	R^2	0.998

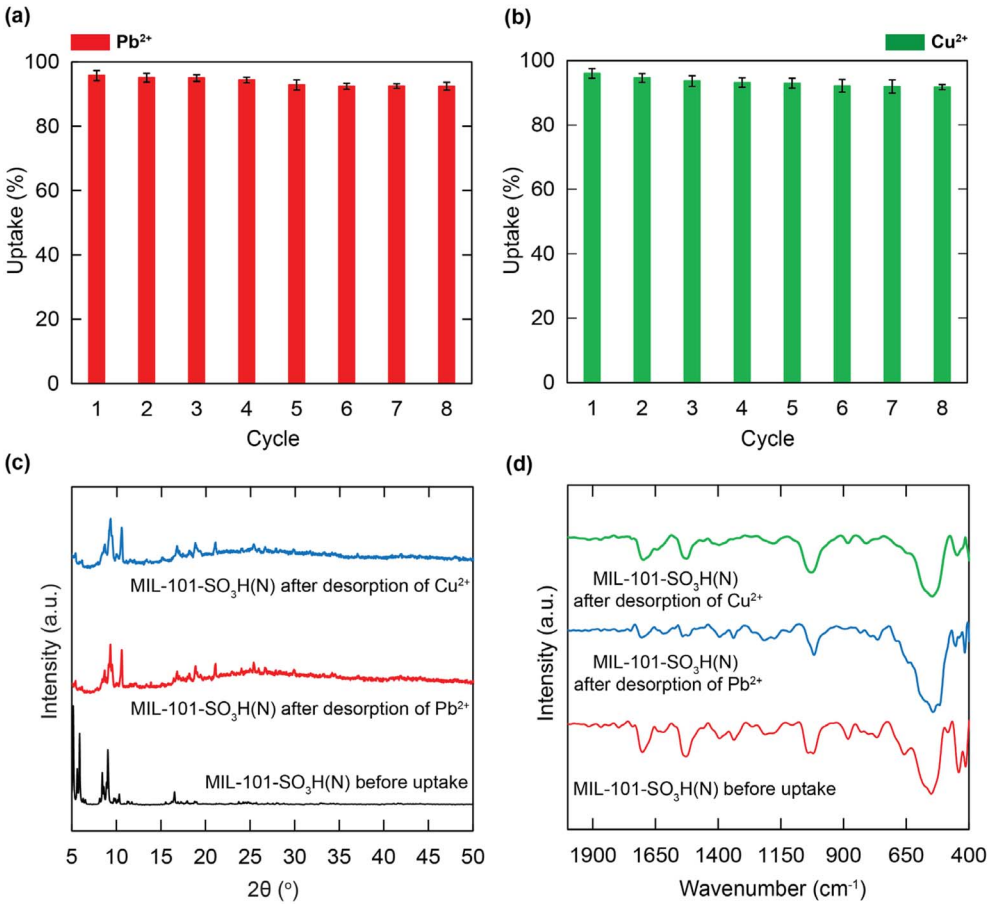

Fig. 7 The reusability of MIL-101-SO_3H(N) in Pb^{2+} uptake (a), and in Cu^{2+} uptake (b); the PXRD analysis of MIL-101-SO_3H(N) before uptake (black) in comparison with the PXRD pattern of MIL-101-SO_3H(N) after desorption of Pb^{2+} (red), and Cu^{2+} (blue) (c); the FT-IR spectra of MIL-101-SO_3H(N) before uptake (red) and after desorption of Pb^{2+} (blue) and Cu^{2+} (green) (d).

Table 3 The maximum adsorption capacity of Pb^{2+} onto MIL-101-SO_3H(N) in comparison with other materials

Adsorption of Pb^{2+}			
Materials	q_{max} (mg g^{-1})	pH	Ref.
VNU-23	617.3	5.5	48
MIL-101(Cr)-NH_2	88.0	6.0	56
Tb-MOFs	547.0	5.5	62
Active carbon	43.9	5.7	66
MoS_2 biochar	189	5.0	67
UiO-66-$(COOH)_2$	420.2	4.8	68
HCMUE-2	1115.9	5.5	69
Fe-MIL-88NH_2	106.0	7.0	70
COF-NHOH	368.7	5.0	71
COF-SH	239.0	5.0	72
Mn-Goethite 4	90.1	5.0	73
Fe_3O_4-SO_3H	108.9	7.0	74
MIL(Cr)-Z1	102.7	5.0	**This study**
MIL-101-SO_3H(N)	**1449.7**	**5.5**	

significant change as compared to the material before Pb^{2+}/Cu^{2+} uptake (Fig. 7d). These data proved that MIL-101-SO_3H(N) could be used as an efficiently reusable adsorbent in removing highly toxic heavy metal ions from wastewater.

To further confirm the features of the MIL-101-SO_3H(N) material, the maximum Pb^{2+}/Cu^{2+} adsorption capacity of the material was compared with those of other adsorbents in Tables 3 and 4. MIL-101-SO_3H(N) has a much higher adsorption

Table 4 The maximum adsorption capacity of Cu^{2+} onto MIL-101-SO_3H(N) in comparison with other materials

Adsorption of Cu^{2+}			
Materials	q_{max} (mg g^{-1})	pH	Ref.
HAP/HA	58.4	5.0	75
MOF-5	290.0	5.2	76
MIL-68(Ga)	130.0	3.0	77
TEPA-MIL-101(Cr)	217.7	6.5	78
$[(Zn_3L_3(H_2O)_6][(Na)(NO_3)]$	379.1	6.0	79
ZIF-8/PAN	275.7	4.0	80
Biochar acrylic-based hydrogel	678.0	6.0	81
ZIF-8	454.7	5.1	82
ZIF-67	617.5	5.2	82
Chitosan-grafted-poly (acrylic acid)	333.3	5.5	83
Natural clays	56.6	5.5	84
MIL(Cr)-Z1	53.3	5.0	**This study**
MIL-101-SO_3H(N)	**1328.4**	**5.0**	

capacity than the other adsorption materials. This can be demonstrated by the sulfonate moieties incorporated and the large pore diameter of the MOF structure, which play an important role in heavy metal ion uptake.

3.8 Plausible uptake mechanism

The ultra-high adsorption performance boosted further investigation into the attraction between the SO_3^- groups inside MIL-101-SO_3H(N) and the Pb^{2+}/Cu^{2+} cations by measurements, including FT-IR and XPS analyses.

It is noteworthy that the FT-IR spectra of Pb⊂MIL-101-SO_3H(N) and Cu⊂MIL-101-SO_3H(N) exhibit shifts to new positions at 533 (517), 1196 (1201), 1384 (1377), and 1611 (1608) cm^{-1}, corresponding to the characteristic modes of Pb–O (Cu–O), SO_3^-, symmetric C–O, and asymmetric C–O, respectively (Fig. S5 and S6†). These findings demonstrate the strong interaction, resulting in the generation of robust chemical bonds between the sulfonate groups and the Pb^{2+}/Cu^{2+} ions and moving the characteristic frequency bands to lower wavenumber regions. This phenomenon has also been observed in previous studies.[48,69] In addition, the adsorption mechanism was further confirmed with the XPS analysis. As shown in Fig. 8a, the XPS spectra of Pb⊂MIL-101-SO_3H(N) and Cu⊂MIL-101-SO_3H(N) indicate the presence of C, O, S, and Cr elements,

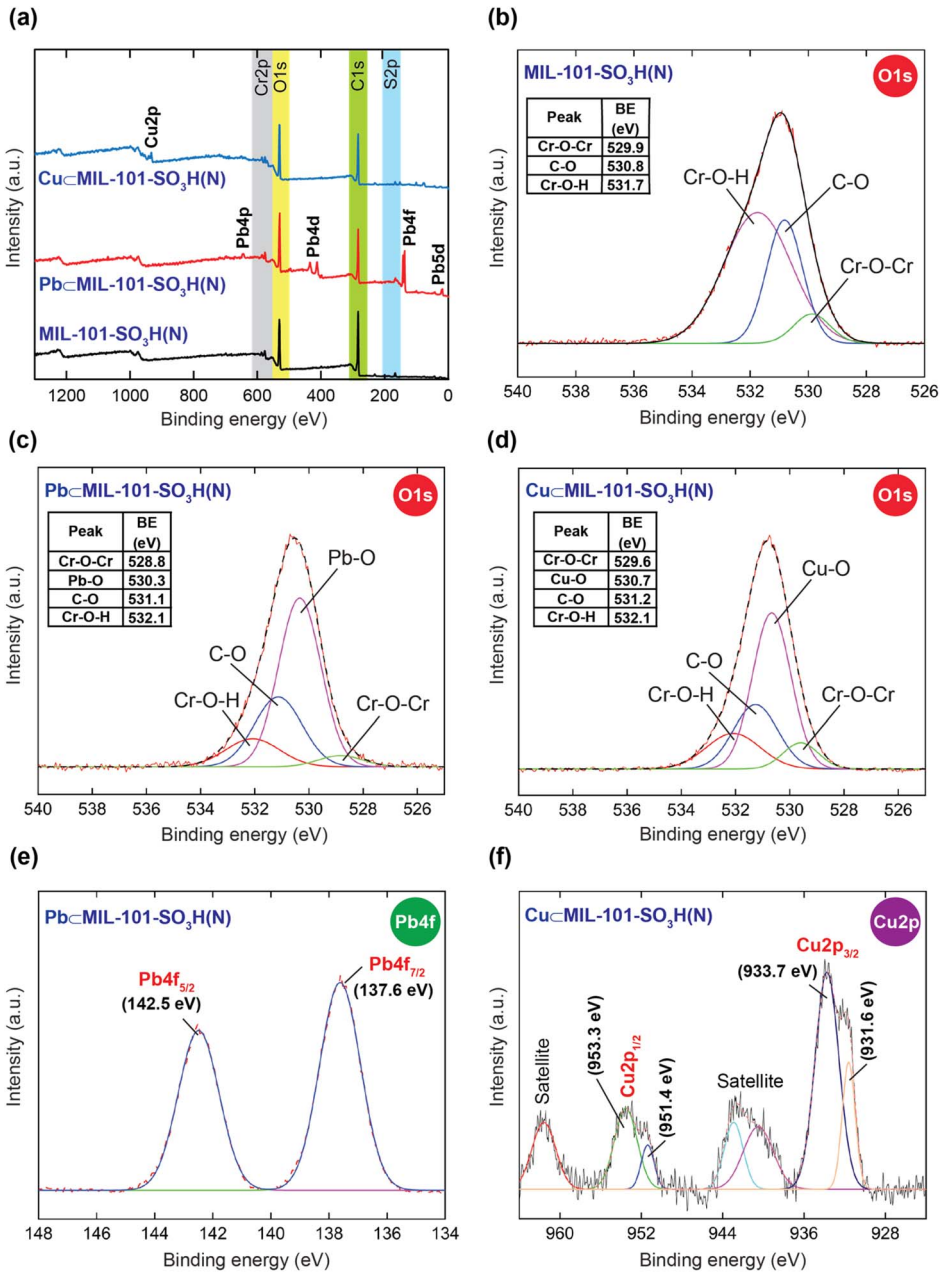

Fig. 8 The XPS measurement of MIL-101-SO_3H(N) before and after Pb^{2+} and Cu^{2+} adsorption: (a) the XPS survey; (b) high-resolution curve of O 1s in MIL-101-SO_3H(N); (c) high-resolution spectrum of O 1s in Pb⊂MIL-101-SO_3H(N); (d) high-resolution spectrum of O 1s in Cu⊂MIL-101-SO_3H(N); (e) the Pb 4f XPS spectrum in Pb⊂MIL-101-SO_3H(N); (f) the Cu 2p XPS spectrum in Cu⊂MIL-101-SO_3H(N).

consistent with the MIL-101-SO_3H(N) spectrum. In detail, new different peaks appeared at 20.5, 138.5, 433.8, and 642.6 eV, corresponding to Pb 5d, Pb 4f, Pb 4d, and Pb 4p, respectively, in the Pb⊂MIL-101-SO_3H(N) spectrum. Meanwhile, in the Cu⊂MIL-101-SO_3H(N) spectrum, there is a new peak at 933.3 eV, corresponding to the Cu 2p signal within the material, indicating that MIL-101-SO_3H(N) efficiently captured the Pb^{2+}/Cu^{2+} cations over the MOF backbone. Next, the O 1s spectra of Pb⊂MIL-101-SO_3H(N) (Cu⊂MIL-101-SO_3H(N)) are divided into four characteristic peaks located at 528.8 (529.6), 530.3 (530.7), 531.1 (531.2), and 532.1 (532.1) eV, which are assigned to the Cr–O–Cr, Pb–O (Cu–O), C–O, and Cr–O–H bonds (Fig. 8c and d).[48,59] It is interesting to note that these peaks move to various binding energy ranges as compared to MIL-101-SO_3H(N), such as 529.9 eV for Cr–O–Cr, 530.8 eV for C–O, and 531.7 eV for Cr–O–H (Fig. 8b).[48,59] Furthermore, the Pb–O and Cu–O peaks are not present in the O 1s curve of MIL-101-SO_3H(N). This can be explained by the strong interaction between the heavy metal cations and the adsorption sites within the framework. Considerably, the high-resolution band of Pb 4f in the Pb⊂MIL-101-SO_3H(N) sample is separated into signals at 137.6 and 142.5 eV, corresponding to Pb $4f_{7/2}$ and Pb $4f_{5/2}$, respectively. Similarly, the Cu 2p high-resolution spectrum is deconvoluted into peaks at 931.6 and 933.7 eV for Cu $2p_{3/2}$, and at 951.4 and 953.3 eV for Cu $2p_{1/2}$, along with the satellite peaks of Cu⊂MIL-101-SO_3H(N). The Pb 4f and Cu 2p peaks have different signals compared with the pure solution of Pb^{2+} and Cu^{2+}.[64,68,85] This further strengthens the explanation that the O species originating from the sulfonic groups, μ-OH-containing clusters, and COO^- in the linkers within the MOF structure can effectively coordinate with the Pb^{2+} and Cu^{2+} ions to create metal-oxo bonds.

4 Conclusion

In summary, a new MIL-101-type Cr-based MOF incorporating a large number of sulfonic moieties and having a suitable pore diameter was fabricated and investigated for its uptake performance for Pb^{2+} and Cu^{2+} cations. Accordingly, MIL-101-SO_3H(N) exhibited the highest adsorption capacity for the heavy metal ions, reaching 1449.7 mg g^{-1} for Pb^{2+} and 1328.4 mg g^{-1} for Cu^{2+} at an optimal pH value. To the best of our knowledge, these values are much larger than those of other adsorbents reported for capturing highly toxic heavy metal ions. Additionally, the uptake of Pb^{2+} and Cu^{2+} occurs *via* chemisorption, as evidenced by the good agreement with the Langmuir isotherm and pseudo-second-order kinetic models. Furthermore, regeneration experiments reveal that Pb^{2+} and Cu^{2+} adsorption is maintained for at least eight consecutive cycles without any significant loss in efficiency. Notably, the uptake mechanism is elucidated through combined modern techniques. All achieved data exhibit that the adsorption mechanism can be confirmed by the formation of strong chemical attraction through the electrostatic interaction of the sulfonate groups located in the MOF backbone and the metal cations. These observations affirm that the sulfonic-modified Cr-based MOF is a potential adsorbent in removing Pb^{2+} and Cu^{2+} ions from wastewater. In addition, the structural order of sulfonic-based MOFs is lost upon activation due to the high flexibility of SO_3H groups. Therefore, future research should focus on immobilizing sulfonic moieties through functional group incorporation to form a rigid backbone for applications in the gaseous phase, as well as comprehensively evaluating the competition of other ions during Pb^{2+} and Cu^{2+} uptake.

Data availability

Data available on request from the corresponding author.

Author contributions

M. V. N. formulated this project. M. V. N., H. K. D., T. M. N., L. C. L., and H. N. N. prepared the materials and collected the PXRD, FT-IR and Raman spectra, and TGA/DSC curves. M. V. N. analyzed all experimental data. M. V. N. wrote the paper and all authors contributed to revising it. All authors have approved the final version of the manuscript.

Conflicts of interest

The authors maintain that they have no conflict of interest for this communication.

Acknowledgements

This research is funded by Ho Chi Minh City University of Education Foundation for Science and Technology under grant number CS.2024.19.57.

Notes and references

1 H. A. Sani, M. B. Ahmada and T. A. Saleh, Synthesis of zinc oxide/talc nanocomposite for enhanced lead adsorption from aqueous solutions, *RSC Adv.*, 2016, **6**, 108819–108827.
2 A. R. Mahdavian and M. A. S. Mirrahimi, Efficient separation of heavy metal cations by anchoring polyacrylic acid on superparamagnetic magnetite nanoparticles through surface modification, *Chem. Eng. J.*, 2010, **159**, 264–271.
3 C. Chen, F. Wei, L. Ye, Y. Wang, L. Long, C. Xu, Y. Xiao, J. Wu, M. Xu, J. He and G. Yang, Adsorption of Cu^{2+} by UV aged polystyrene in aqueous solution, *Ecotoxicol. Environ. Saf.*, 2022, **232**, 113292.
4 M. Ramezanpour, A. R. Shirin-Abadi and M. Enayati, Adsorption study of Cu^{2+} by using CO_2/electric potential-responsive polymeric monoliths prepared by medium internal phase emulsion, *ACS Appl. Polym. Mater.*, 2024, **6**, 10311–10321.
5 D. Fan, Y. Peng, X. He, J. Ouyang, L. Fu and H. Yang, Recent progress on the adsorption of heavy metal ions Pb (II) and Cu (II) from wastewater, *Nanomaterials*, 2024, **14**, 1037.
6 N. Abdullah, R. J. Gohari, N. Yusof, A. F. Ismail, J. Juhana, W. J. Lau and T. Matsuura, Polysulfone/hydrous ferric oxide ultrafiltration mixed matrix membrane: preparation,

characterization and its adsorptive removal of lead (II) from aqueous solution, *Chem. Eng. J.*, 2016, **289**, 28–37.
7 C. Liu, R. Bai and Q. S. Ly, Selective removal of copper and lead ions by diethylenetriamine-functionalized adsorbent: behaviors and mechanisms, *Water Res.*, 2008, **42**, 1511–1522.
8 M. Naushad, T. Ahamad, B. M. Al-Maswari, A. Abdullah Alqadami and S. M. Alshehri, Nickel ferrite bearing nitrogen-doped mesoporous carbon as efficient adsorbent for the removal of highly toxic metal ion from aqueous medium, *Chem. Eng. J.*, 2017, **330**, 1351–1360.
9 Q. Dong, X. Guo, X. Huang, L. Liu, R. Tallon, B. Taylor and J. Chen, Selective removal of lead ions through capacitive deionization: role of ion-exchange membrane, *Chem. Eng. J.*, 2021, **369**, 1535–1542.
10 J. Qian, Z. Zeng, W. Xue and Q. Guo, Lead removal from aqueous solutions by 732 cation-exchange resin, *Can. J. Chem. Eng.*, 2015, **94**, 142–150.
11 Y. Guo, H. Feng, L. Zhang, Y. Wu, C. Lan, J. Tang, J. Wang and L. Tang, Insights into the mechanism of selective removal of heavy metal ions by the pulsed/direct current electrochemical method, *Environ. Sci. Technol.*, 2024, **58**, 5589–5597.
12 D. Kavak, Removal of lead from aqueous solutions by precipitation: statistical analysis and modeling, *Desalin. Water Treat.*, 2013, **51**, 1720–1726.
13 L. Largitte, S. Gervelas, T. Tant, P. Couespel Dumesnil, A. Hightower, R. Yasami, Y. Bercion and P. Lodewyckx, Removal of lead from aqueous solutions by adsorption with surface precipitation, *Adsorption*, 2014, **20**, 689–700.
14 J. Di, Z. Ruan, S. Zhang, Y. Dong, S. Fu, H. Li and G. Jiang, Adsorption behaviors and mechanisms of Cu^{2+}, Zn^{2+} and Pb^{2+} by magnetically modified lignite, *Sci. Rep.*, 2022, **12**, 1394.
15 Y. Xiao, M. Sun, L. Zhang, X. Gao, J. Su and H. Zhu, The co-adsorption of Cu^{2+} and Zn^{2+} with adsorption sites surface-lattice reforming on calcined layered double hydroxides, *RSC Adv.*, 2015, **5**, 28369–28378.
16 L. Huang, X. Weng, Z. Chen, M. Megharaj and R. Naidu, Green synthesis of iron nanoparticles by various tea extracts: comparative study of the reactivity, *Spectrochim. Acta, Part A*, 2014, **130**, 295–301.
17 N. Wang, Y. F. Wang, A. M. Omer and X. K. Ouyang, Fabrication of novel surface-imprinted magnetic graphene oxide-grafted cellulose nanocrystals for selective extraction and fast adsorption of fluoroquinolones from water, *Anal. Bioanal. Chem.*, 2017, **409**, 6643–6653.
18 T. M. Alslaibi, I. Abustan, M. A. Ahmad and A. A. Foul, A review: production of activated carbon from agricultural by products via conventional and microwave heating, *J. Chem. Technol. Biotechnol.*, 2013, **88**, 1183–1190.
19 P. Tan, J. Sun, Y. Hu, Z. Fang, Q. Bi, Y. Chen and J. Cheng, Adsorption of Cu^{2+}, Cd^{2+} and Ni^{2+} from aqueous single metal solutions on graphene oxide membranes, *J. Hazard. Mater.*, 2015, **297**, 251–260.
20 C. Hao and A. Wang, Adsorption of Cu^{2+}, Ni^{2+}, and Cr (VI) heavy metal ions on sodium hexatitanate nanorods from industrial electroplating wastewater assisted by calcium hypochlorite oxidation, *Ind. Eng. Chem. Res.*, 2024, **63**, 16990–17005.
21 T. D. N. Phan, V. H. Pham, E. W. Shin, H. D. Pham, S. Kim, J. S. Chung, E. J. Kim and S. H. Hur, The role of graphene oxide content on the adsorption-enhanced photocatalysis of titanium dioxide/graphene oxide composites, *Chem. Eng. J.*, 2011, **170**, 226–232.
22 D. Kołodyńska, J. Krukowska and P. Thomas, Comparison of sorption and desorption studies of heavy metal ions from biochar and commercial active carbon, *Chem. Eng. J.*, 2017, **307**, 353–363.
23 A. M. Al-Ma'abreh, D. A. Hmedat, G. Edris and M. A. Hamed, Removal of heavy metal ions (Pb^{2+}, Co^{2+}, and Cd^{2+}) by activated carbon from cypress fruit: an investigation of kinetics, thermodynamics, and isotherms, *J. Chem.*, 2024, 1984821.
24 J. Du, A. Zhou, X. Lin and Y. Bu, Adsorption mechanism of Pb^{2+} in montmorillonite nanopore under various temperatures and concentrations, *Environ. Res.*, 2022, **209**, 112817.
25 X. Lu, F. Wang, X. Y. Li, K. Shih and E. Y. Zeng, Adsorption and thermal stabilization of Pb^{2+} and Cu^{2+} by zeolite, *Ind. Eng. Chem. Res.*, 2016, **55**, 8767–8773.
26 E. Feldbusch, J. Zotzmann, V. Roddatis, K. Dideriksen, R. Blukis, A. Schleicher and S. Regenspurg, Removal of Pb^{2+} and Cu^{2+} from artificial geothermal brine by zeolite at various salinity and temperature conditions, *Appl. Geochem.*, 2024, **175**, 106157.
27 K. H. H. Aziz, F. S. Mustafa and S. Hama, Pharmaceutical removal from aquatic environments using multifunctional metal-organic frameworks (MOFs) materials for adsorption and degradation processes: a review, *Coord. Chem. Rev.*, 2025, **542**, 216875.
28 K. H. H. Aziz, F. S. Mustafa, R. F. Hamarawf and K. M. Omer, Adsorptive removal of toxic heavy metals from aquatic environment by metal organic framework (MOF): a review, *J. Water Process Eng.*, 2025, **70**, 106867.
29 K. H. H. Aziz and R. Kareem, Recent advances in water remediation from toxic heavy metals using biochar as a green and efficient adsorbent: a review, *Case Stud. Chem. Environ. Eng.*, 2023, **8**, 100495.
30 H. Furukawa, K. E. Cordova, M. O'Keeffe and O. M. Yaghi, The chemistry and applications of metal-organic frameworks, *Science*, 2013, **341**, 1230444.
31 H. C. Zhou, J. R. Long and O. M. Yaghi, Introduction to metal-organic frameworks, *Chem. Rev.*, 2012, **112**, 673–674.
32 D. T. Nguyen, H. N. Nguyen, T. M. Nguyen, H. C. Dong, N. N. Dang, Q.-H. Tran, T. A. Nguyen, M. V. Tran, T. L. H. Doan, L. C. Luu and M. V. Nguyen, An excellent photodegradation efficiency of methylene blue and rhodamine B dyes in a series of porphyrinic aluminum-based MOFs metallated by copper and cobalt metals, *Colloids Surf., A*, 2024, **689**, 133663.
33 M. V. Nguyen, H. C. Dong, V. T. N. Truong, H. N. Nguyen, L. C. Luu, N. N. Dang and T. A. T. Nguyen, A new porphyrinic vanadium-based MOF constructed from infinite $V(OH)O_4$ chains: syntheses, characterization and

photoabsorption properties, *New J. Chem.*, 2022, **46**, 632–641.

34 T. T. M. Bui, L. T. Nguyen, N. P. H. Pham, C. C. Tran, L. T. Nguyen, T. A. Nguyen, H. N. Nguyen and M. V. Nguyen, A new approach for ultra-high adsorption of cationic methylene blue in a Zr-sulfonic-based metal-organic framework, *RSC Adv.*, 2021, **11**, 36626–36635.

35 K. M. V. Nguyen, A. V. N. Phan, N. T. Dang, T. Q. Tran, H. K. Duong, H. N. Nguyen and M. V. Nguyen, Efficiently improving the adsorption capacity of the rhodamine B dye in a SO_3H-functionalized chromium-based metal-organic framework, *Adv. Mater.*, 2023, **4**, 2636–2647.

36 L. E. Kreno, K. Leong, O. K. Farha, M. Allendorf, R. P. V. Duyne and J. T. Hupp, Metal-organic framework materials as chemical sensors, *Chem. Rev.*, 2012, **112**, 1105–1125.

37 M. V. Nguyen, T. U. Kim, L. H. T. Nguyen, A. Mirzaei, A. T. T. Pham, T. Q. Tran, N. X. D. Mai, N. Q. Tran, Y. Kim, T. B. Phan, H. W. Kim, S. S. Kim and T. L. H. Doan, Efficient low-temperature detection of CO gas by various metalated porphyrinic-Al-based MOF (Cu and Co) materials, *Sens. Actuators, B*, 2025, **424**, 136915.

38 Y. Chen, Y. Zhang, Q. Huang, X. Lin, A. Zeb, Y. Wu, Z. Xu and X. Xu, Recent advances in Cu-based metal-organic frameworks and their derivatives for battery applications, *ACS Appl. Energy Mater.*, 2022, **5**, 7842–7873.

39 M. V. Nguyen, T. B. Phan, M. V. Tran, T. A. T. Nguyen and H. N. Nguyen, A confinement of N-heterocyclic molecules in a metal-organic framework for enhancing significant proton conductivity, *RSC Adv.*, 2022, **12**, 355–364.

40 L. Joseph, M. Saha, S. Kim, B. M. Jun, J. Heo, C. M. Park, M. Jang, J. R. V. Flora and Y. Yoon, Removal of Cu^{2+}, Cd^{2+}, and Pb^{2+} from aqueous solution by fabricated MIL-100(Fe) and MIL-101(Cr): experimental and molecular modeling study, *J. Environ. Chem. Eng.*, 2021, **9**, 106663.

41 X. Zhao, Y. Wang, Y. Li, W. Xue, J. Li, H. Wu, Y. Zhang, B. Li, W. Liu, Z. Gao and H. Huang, Synergy effect of pore structure and amount of carboxyl site for effective removal of Pb^{2+} in metal-organic frameworks, *J. Chem. Eng. Data*, 2019, **64**, 2728–2735.

42 V. Subramaniyam, T. D. Thangadurai and Y. I. Lee, Zirconium based metal-organic framework for the adsorption of Cu(II) ions in real water samples, *Clean. Eng. Technol.*, 2022, **9**, 100526.

43 A. Kumar, K. Kumar, K. Kaur, K. Arya, S. K. Mehta, S. Singh and R. Kataria, Zn-MOF@rGO nanocomposite: a versatile tool for highly selective and sensitive detection of Pb^{2+} and Cu^{2+} ions in water, *Anal. Methods*, 2024, **16**, 6020–6029.

44 I. Sharma, A. Kumar, K. Arya, S. Mehra, A. Kumar, S. K. Mehta and R. Kataria, Dual-functional luminescent Zn-MOF@ MCHS nanocomposite for TNP detection and copper (II) adsorptive removal, *Sep. Purif. Technol.*, 2025, **355**, 129538.

45 K. Arya, A. Kumar, S. Mehra, A. Kumar, S. K. Mehta and R. Kataria, Exploration and removal of multiple metal ions using mixed-linker-architected Zn-MOF in aqueous media, *Sep. Purif. Technol.*, 2023, **307**, 122551.

46 A. Kumar, R. Mehta, S. Kumar, S. K. Sharma, R. Gaba and R. Kataria, Mixed-ligand-based luminescent MOFs as chemical sensors for toxic environmental contaminants, *J. Mol. Struct.*, 2024, **1325**, 140898.

47 A. Kumar, K. Arya, S. Mehra, A. Kumar, S. K. Mehta and R. Kataria, Detection and sorption of heavy metal ions in aqueous media using Zn-based luminescent metal-organic framework, *Sep. Purif. Technol.*, 2024, **333**, 125875.

48 C. C. Tran, H. C. Dong, V. T. N. Truong, T. T. M. Bui, H. N. Nguyen, T. A. T. Nguyen, N. N. Dang and M. V. Nguyen, Enhancing the remarkable adsorption of Pb^{2+} in a series of sulfonic-functionalized Zr-based MOFs: a combined theoretical and experimental study for elucidating the adsorption mechanism, *Dalton Trans.*, 2022, **51**, 7503–7516.

49 G. Wang, G. Xiao and D. Yan, Synthesis and properties of soluble sulfonated polybenzimidazoles derived from asymmetric dicarboxylic acid monomers with sulfonate group as proton exchange membrane, *J. Membr. Sci.*, 2011, **369**, 388–396.

50 Z. Niu, S. Zhang, M. Ma, Z. Wang, H. Zhao and Y. Wang, Synthesis of novel waste batteries-sawdust-based adsorbent via a two-stage activation method for Pb^{2+} removal, *Environ. Sci. Pollut. Res.*, 2019, **26**, 4730–4745.

51 X. Yang, S. Yang, S. Yang, J. Hu, X. Tan and X. Wang, Effect of pH, ionic strength and temperature on sorption of Pb(II) on NKF-6 zeolite studied by batch technique, *Chem. Eng. J.*, 2011, **168**, 86–93.

52 R. R. Sheha, Preparation and performance of a novel composite as a reactive resin for copper retention, *Chem. Eng. J.*, 2012, **213**, 163–174.

53 M. Zhu, P. Hu, Z. Tong, Z. Zhao and Z. Zhao, Enhanced hydrophobic MIL (Cr) metal-organic framework with high capacity and selectivity for benzene VOCs capture from high humid air, *Chem. Eng. J.*, 2017, **313**, 1122–1131.

54 Y. He, Z. Shan, T. Tan, Z. Chen and Y. Zhang, Ternary sulfur/polyacrylonitrile/SiO_2 composite cathodes for high-performance sulfur/lithium ion full batteries, *Polymers*, 2018, **10**, 930.

55 X. Wang and Y. Li, Nanoporous carbons derived from MOFs as metal-free catalysts for selective aerobic oxidations, *J. Mater. Chem. A*, 2016, **4**, 5247–5257.

56 X. Luo, L. Ding and J. Luo, Adsorptive removal of Pb(II) ions from aqueous samples with amino-functionalization of metal-organic frameworks MIL-101-Cr, *J. Chem. Eng. Data*, 2015, **60**, 1732–1743.

57 L. Ma, L. Xu, H. Jiang and X. Yuan, Comparative research on three types of MIL-101 (Cr)-SO_3H for esterification of cyclohexene with formic acid, *RSC Adv.*, 2019, **9**, 5692–5700.

58 Y. He, W. Dong, X. Li, D. Wang, Q. Yang, P. Deng and J. Huang, Modified MIL-100(Fe) for enhanced photocatalytic degradation of tetracycline under visible-light irradiation, *J. Colloid Interface Sci.*, 2020, **574**, 364–376.

59 T. K. Vo, J. H. Kim, H. T. Kwon and J. Kim, Cost-effective and eco-friendly synthesis of MIL-101 (Cr) from waste hexavalent chromium and its application for carbon monoxide separation, *J. Ind. Eng. Chem.*, 2019, **80**, 345–351.

60 C. S. Nkutha, P. N. Diagboya, F. M. Mtunzi and E. D. Dikio, Application of eco-friendly multifunctional porous graphene oxide for adsorptive sequestration of chromium in aqueous solution, *Water Environ. Res.*, 2020, **92**, 1070–1079.
61 D. Chen, W. Shen, S. Wu, C. Chen, X. Luo and L. Guo, Ion exchange induced removal of Pb(II) by MOF-derived magnetic inorganic sorbents, *Nanoscale*, 2016, **8**, 7172–7179.
62 H. Zhu, J. Yuan, X. Tan, W. Zhang, M. Fang and X. Wang, Efficient removal of Pb^{2+} by Tb-MOFs: identifying the adsorption mechanism through experimental and theoretical investigations, *Environ. Sci.: Nano*, 2019, **6**, 261–272.
63 M. V. Nguyen, H. N. Nguyen, T. A. Nguyen and K. M. V. Nguyen, Engineering of appropriate pore size combined with sulfonic functionalization in a Zr-MOF with reo topology for the ultra-high removal of cationic malachite green dye from an aqueous medium, *RSC Adv.*, 2022, **12**, 30201–30212.
64 C. X. Yu, K. Z. Wang, X. J. Li, D. Liu, L. F. Ma and L. L. Liu, Highly efficient and facile removal of Pb^{2+} from water by using a negatively charged azoxy-functionalized metal-organic framework, *Cryst. Growth Des.*, 2020, **20**, 5251–5260.
65 H. Wang, D. B. Jiang, J. Gu, L. Ouyang, Y. X. Zhang and S. Yuan, Simultaneous removal of phenol and Pb^{2+} from the mixed solution by zwitterionic poly(sulfobetaine methacrylate)-grafted PVBC microspheres, *Ind. Eng. Chem. Res.*, 2020, **59**, 6065–6077.
66 J. Acharyaa, J. N. Sahu, C. R. Mohanty and B. C. Meikap, Removal of lead(II) from wastewater by activated carbon developed from Tamarind wood by zinc chloride activation, *Chem. Eng. J.*, 2009, **149**, 249–262.
67 H. Zhu, X. Tan, L. Tan, C. Chen, N. S. Alharbi, T. Hayat, M. Fang and X. Wang, Biochar derived from sawdust embedded with molybdenum disulfide for highly selective removal of Pb^{2+}, *ACS Appl. Nano Mater.*, 2018, **1**, 2689–2698.
68 X. Zhao, Y. Wang, Y. Li, W. Xue, J. Li, H. Wu, Y. Zhang, B. Li, W. Liu, Z. Gao and H. Huang, Synergy effect of pore structure and amount of carboxyl site for effective removal of Pb^{2+} in metal-organic frameworks, *J. Chem. Eng. Data*, 2019, **64**, 2728–2735.
69 H. M. N. Pham, A. V. N. Phan, A. N. T. Phan, V. P. Nguyen, K. M. V. Nguyen, H. N. Nguyen, T. M. Nguyen and M. V. Nguyen, Engineering of efficient functionalization in a zirconium-hydroxyl-based metal-organic framework for an ultra-high adsorption of Pb^{2+} ions from an aqueous medium: an elucidated uptake mechanism, *Adv. Mater.*, 2024, **5**, 5118–5133.
70 Q. Fu, J. Lou, L. Peng, R. Zhang, S. Zhou, P. Wu, W. Yan, C. Mo and J. Luo, Iron based metal organic framework for efficient removal of Pb^{2+} from wastewater, *J. Solid State Chem.*, 2021, **300**, 122188.
71 D. Xiang, R. Zhu, Y. Chen, M. Zhu, S. Wang, Y. Wu, J. Luo and L. Fu, Preparation of amidoxime modified covalent organic framework for efficient adsorption of lead ions in aqueous solution, *Chem. Eng. J.*, 2024, **492**, 152292.
72 Y. Cao, X. Hu, C. Zhu, S. Zhou, R. Li, H. Shi, S. Miao, M. Vakili, W. Wang and D. Qi, Sulfhydryl functionalized covalent organic framework as an efficient adsorbent for selective Pb (II) removal, *Colloids Surf., A*, 2020, **600**, 125004.
73 H. Liu, X. Lu, M. Li, L. Zhang, C. Pan, J. Li, R. Zhang and W. Xiang, Structural incorporation of manganese into goethite and its enhancement of Pb (II) adsorption, *Environ. Sci. Technol.*, 2018, **52**, 4719–4727.
74 K. Chen, J. He, Y. Li, X. Cai, K. Zhang, T. Liu, Y. Hu, D. Lin, L. Kong and J. Liu, Removal of cadmium and lead ions from water by sulfonated magnetic nanoparticle adsorbents, *J. Colloid Interface Sci.*, 2017, **494**, 307–316.
75 L. Yang, Z. Wei, W. Zhong, J. Cui and W. Wei, Modifying hydroxyapatite nanoparticles with humic acid for highly efficient removal of Cu(II) from aqueous solution, *Colloids Surf., A*, 2016, **490**, 9–21.
76 N. Bakhtiari and S. Azizian, Adsorption of copper ion from aqueous solution by nanoporous MOF-5: a kinetic and equilibrium study, *J. Mol. Liq.*, 2015, **206**, 114–118.
77 Y. Zhang, L. Liu, D. Yu, J. Liu, L. Zhao, J. Liu and S. Liu, Preparation of magnetic MIL-68(Ga) metal–organic framework and heavy metal ion removal application, *Molecules*, 2022, **27**(11), 1–10.
78 N. Rastkari, S. Akbari, M. B. Brahmand, A. Takhvar and R. Ahmadkhaniha, Synthesis and characterization of tetraethylene pentamine functionalized MIL-101(Cr) for removal of metals from water, *J. Environ. Health Sci. Eng.*, 2021, **19**, 1735–1742.
79 C. Yu, Z. Shao, L. Liu and H. Hou, Efficient and selective removal of copper (II) from aqueous solution by a highly stable hydrogen-bonded metal-organic framework, *Cryst. Growth Des.*, 2018, **18**, 3082–3088.
80 H. Zhang, R. Li, H. Xu, L. Quan, C. Zhan, P. Han, K. Xu and Y. Tong, Mechanism insights into high-performance Cu^{2+} adsorption by ZIF-8/PAN nanocomposite fibers: coordination and ion exchange dynamics, *Polym. Adv. Technol.*, 2025, **36**, e70068.
81 X. Fan, X. Wang, Y. Cai, H. Xie, S. Han and C. Hao, Functionalized cotton charcoal/chitosan biomass-based hydrogel for capturing Pb^{2+}, Cu^{2+} and MB, *J. Hazard. Mater.*, 2022, **423**, 127191.
82 Y. Huang, X. Zeng, L. Guo, J. Lan, L. Zhang and D. Cao, Heavy metal ion removal of wastewater by zeolite-imidazolate frameworks, *Sep. Purif. Technol.*, 2018, **194**, 462–469.
83 X. Wang, Y. Zheng and A. Wang, Fast removal of copper ions from aqueous solution by chitosan-g-poly (acrylic acid)/attapulgite composites, *J. Hazard. Mater.*, 2009, **168**, 970–977.
84 T. B. Musso, M. E. Parolo, G. Pettinari and F. M. Francisca, Cu (II) and Zn (II) adsorption capacity of three different clay liner materials, *J. Environ. Manage.*, 2014, **146**, 50–58.
85 M. Ganiga and J. Cyriac, Understanding the photoluminescence mechanism of nitrogen-doped carbon dots by selective interaction with copper ions, *ChemPhysChem*, 2016, **17**, 2315–2321.